Gao *et al. Microstructures* 2022;2:2022010
DOI: 10.20517/microstructures.2022.03

Microstructures

Research Article

Open Access

Check for updates

An intriguing canting dipole configuration and its evolution under an electric field in La-doped $Pb(Zr,Sn,Ti)O_3$ perovskites

Botao Gao[1,2], Hui Liu[1,3], Zhengyang Zhou[2], Ke Xu[4], He Qi[1,3], Shiqing Deng[1,3], Yang Ren[5], Junliang Sun[6], Houbing Huang[4], Jun Chen[1,3]

[1]Beijing Advanced Innovation Center for Materials Genome Engineering, Department of Physical Chemistry, University of Science and Technology Beijing, Beijing 100083, China.
[2]Shanghai Institute of Ceramics, Chinese Academy of Sciences, Shanghai 201899, China.
[3]School of Mathematics and Physics, University of Science and Technology Beijing, Beijing 100083, China.
[4]School of Materials Science and Engineering, Beijing Institute of Technology, Beijing 100081, China.
[5]X-Ray Science Division, Advanced Photon Source, Argonne National Laboratory, Argonne, Illinois 60439, USA.
[6]College of Chemistry and Molecular Engineering, Peking University, Beijing 100871, China.

Correspondence to: Prof./Dr. Jun Chen, Beijing Advanced Innovation Center for Materials Genome Engineering, Department of Physical Chemistry, University of Science and Technology Beijing, No. 30 Xueyuan Road, Haidian District, Beijing 100083, China. E-mail: junchen@ustb.edu.cn

How to cite this article: Gao B, Liu H, Zhou Z, Xu K, Qi H, Deng S, Ren Y, Sun J, Huang H, Chen J. An intriguing canting dipole configuration and its evolution under an electric field in La-doped $Pb(Zr,Sn,Ti)O_3$ perovskites. *Microstructures* 2022;2:2022010. https://dx.doi.org/10.20517/microstructures.2022.03

Received: 1 Mar 2022 **First Decision:** 18 Mar 2022 **Revised:** 28 Mar 2022 **Accepted:** 1 Apr 2022 **Published:** 18 Apr 2022

Academic Editor: Zibin Chen **Copy Editor:** Peng-Juan Wen **Production Editor:** Peng-Juan Wen

Abstract

Despite the fact that electric dipole ordering plays a key role in the unique physical properties of dielectric materials, electric dipole configurations mostly appear simply as either parallel or antiparallel. Here, we report a canting electric dipole configuration in La-doped $Pb(Zr,Sn,Ti)O_3$ perovskites based on advanced neutron, synchrotron X-ray and three-dimensional electron diffraction techniques. It is revealed that, arising from the coupling between the atomic displacement and oxygen octahedral tilting, this unique electric dipole configuration displays a canting arrangement aligned in the $(110)_p$ plane that possesses an antiparallel component along the $[110]_p$ direction and a parallel component along the $[001]_p$ direction. Remarkably, under an *in-situ* electric field, the electric dipoles continuously rotate with a gradually reduced canting angle, as confirmed by phase-field simulations, and ultimately evolve into a ferroelectric ordering. Such an evolution gives rises to a small hysteresis and an equivalent lattice strain to the macroscopic strain. These findings enrich the current understanding of the types of electric dipole configurations in dielectric materials and are expected to aid the design of new dielectric

materials with emergent properties.

Keywords: Antiferroelectric, electric dipole configurations, canting, perovskite

INTRODUCTION

The breaking of time-reversal symmetry results in magnetic dipoles and the formation of magnetic functional materials. The presence of electric dipoles arising from the breaking of space inversion symmetry is responsible for the rich functionalities of dielectric materials[1]. The alignment of these dipoles synergistically with the crystal lattice governs their defining physical properties. Parallel magnetic moments and electric dipole alignments give rise to ferromagnetism and ferroelectricity (FE), respectively, while the antiparallel equivalents can be termed as antiferromagnetism (AFM) and antiferroelectricity (AFE). In addition to these simple collinear configurations of magnetic moments, many complex non-collinear ones have been found, including cycloidal[2], helicoidal[3], canting[4], conical[5], spin spirals[6], spin-density waves[7] and skyrmions[8,9]. Such non-collinear magnetic moments can lead to a variety of staggering physical phenomena, such as magnetocaloric[10] and anomalous Hall effects[11], magnetostrictions[12] and negative thermal expansion[13,14]. In contrast, the typical arrangement of electric dipoles seems to be much simpler. Most configurations are parallel or antiparallel collinear configurations, as exemplified by ferroelectric $PbTiO_3$ and antiferroelectric $PbZrO_3$. The non-collinear ordering of electric dipoles has rarely been reported so far[15-18]. Given the fact that electrical properties are governed by electric dipole configurations, the discovery of a new configuration is of great significance for not only understanding the nature of dielectric properties but also for designing new materials.

It is well known that many complex magnetic moment orderings stabilized by the competition between different energy states often manifest in complex commensurate/incommensurate modulated periods in crystal structures[13,14,19]. Similar phenomena have been found in recent studies of dielectric materials. A helical electric dipole ordering has been discovered in the incommensurate ferroelectric $BiCu_xMn_{7-x}O_{12}$ quadruple perovskite[20]. Very recently, both sinusoidal and cycloidal arrangements of electric dipoles have been revealed in $PbZrO_3$-based antiferroelectrics[15,21], which occur as a result of the competing AFE and FE orderings. It is noteworthy that chemically modified $PbZrO_3$-based perovskites present significant structural diversity involving oxygen octahedral distortions/rotations, as evidenced by various commensurate/incommensurate structures from electron diffraction[22-27]. This allows for the existence of different competing exchange interactions. Hence, it is hypothesized that interesting electric dipole configurations could be hidden in $PbZrO_3$-based perovskites.

Herein, we report an example of a canting electric dipole ordering in $PbZrO_3$-based perovskites, and its complex modulated crystal structure is resolved using combined advanced diffraction techniques. In particular, the electric dipole component along the $[110]_p$ direction presents an antiparallel alignment, while the parallel component along the $[001]_p$ direction, resulting in a canting dipole configuration. These electric dipoles are manifested as continuous rotational behavior, where the canting angle of the dipoles decreases and ultimately evolves into the FE ordering by applying an *in-situ* electric field. This microscopic evolution gives rise to a slim macroscopic *P-E* loop, which is analogous to the corresponding canting AFM ordering. Finally, the relationship between the slim *P-E* loop and canting dipole configuration is confirmed by phase-field simulations. These findings enrich our understanding of the types of electric dipole configurations in dielectric materials and reveal the internal mechanism of the formation of AFE hysteresis loops.

METHODS

Materials synthesis

The sample was prepared by a conventional solid-state method. PbO, La_2O_3, ZrO_2, TiO_2 and SnO_2 powders with purities of at least 99% were weighed according to the stoichiometric formula $(Pb_{0.91}La_{0.06})(Zr_{0.42}Sn_{0.40}Ti_{0.18})O_3$ (abbreviated as PLZST). A 2 wt.% excess of PbO was added to compensate for the volatilization of Pb during sintering. The raw powders were ball-milled for 6 h and dried at 105 °C. The mixed powders were calcined at 890 °C for 2 h, followed by grinding in an agate mortar. A 6 wt.% polyvinyl acetate binder was added, and then the powders were pressed into disks of 10 mm diameter and 1 mm thickness at 150 MPa. Finally, the binder was burned out at 550 °C for 2 h, and the pellets were sintered at 1300 °C for 1 h.

Electrical property measurements

For the electrical measurements, the ceramic disks were polished to 0.6 mm in thickness, and Au thin films were sputtered to both sides as electrodes. The *P-E* and *S-E* loops were measured on an aixACCT TF Analyzer 1000 (aixACCT Co., Aachen, Germany) at 1 Hz and room temperature. The voltage waveform used for the measurements was a triangle wave.

Three-dimensional electron diffraction

The three-dimensional (3D) electron diffraction data were collected using transmission electron microscopy (TEM, Tecnai F20, FEI) with a submicron crystal. The selected dataset was collected with a tilt angle range from -45° to 45° and an exposure time of 1 s. The goniometer tilt step was 0.5°. More details are presented in the Supplementary Information.

High-resolution neutron powder and synchrotron X-ray diffraction

The ceramics were crushed into a powder for the high-resolution neutron powder diffraction (HR-NPD) and high-resolution synchrotron X-ray diffraction (HR-SXRD) measurements. HR-NPD (λ = 1.6225 Å) was carried out at the Wombat diffractometer, Australian Centre for Neutron Scattering. HR-SXRD (λ = 0.4499 Å) was measured using the BL44B2 beamline of SPring-8, Japan. All the samples were synthesized under the same conditions.

RESULTS AND DISCUSSION

Typical La^{3+}- or Nb^{5+}-doped Pb(Zr,Sn,Ti)O_3 AFE systems have been intensively studied due to the applicable activated electric field of the AFE-to-FE phase transition and excellent electric properties. Distinguished from structural studies of compositions with low Ti^{4+} and La^{3+} contents that exhibit typical double hysteresis loops, some researchers reduced the hysteresis by increasing the content of La[28,29]. This result is of great significance for the design of materials with low energy loss. This phenomenon also suggests that an interesting dipole configuration is hidden in this small hysteresis AFE. In this work, the representative composition of PLZST located in the region with higher La^{3+} and Ti^{4+} contents, which exhibits a unique slim hysteresis loop[30], was selected to reveal the emergent electric dipole configuration.

It is well known that the electric dipoles of perovskites are attributed to the displacements between the cations and the centroid of the surrounding oxygen polyhedra. Therefore, a precise crystal structure analysis is critical to reveal the electric dipole configuration. Two difficulties should be well resolved for the precise analysis of the crystal structure. One is the establishment of a space group and the other is the determination of the position of the light element oxygen. To resolve such difficulties, a combination of modern structural analysis methods has been performed by taking advantage of 3D electron diffraction (3D ED) , HR-NPD and HR-SXRD. It is known that electron diffraction is always the preferred method to find the symmetry of a new structure. Compared to conventional selective area electron diffraction, 3D ED

can reveal more complete structural information with the help of tomography. Neutron diffraction has an incomparable advantage in determining the position of oxygen. SXRD can improve the accuracy of the structural analysis.

The overview and representative reflection planes of 3D ED are shown in Figure 1A-D. Conventional TEM also shows a similar result [Supplementary Figure 1]. According to symmetry operators (the computer-aided program can be seen in the Supplementary Information), an orthorhombic cell of sqrt(2)a_p × sqrt(2)b_p × 2c_p (Z = 4) can be used to index the whole dataset. The reflection conditions of 3D ED were summarized as: *hkl*: $h + k + l = 2n$; *hk*0: $h + k = 2n$; 0*kl*: $k + l = 2n$; *h*0*l*: h, $l = 2n$, which suggests three possible space groups of *Imam* (non-polar), *Ima*2 or *Ia* (low symmetry). Owing to the non-negligible remnant polarization of the macro property, the polar space group *Ima*2 is reasonable.

To further determine the crystal structure of PLZST, both HR-NPD and HR-SXRD were adopted [Supplementary Figure 2]. Finally, a polar orthorhombic unit cell of *Ima*2 [a_o = 5.77245(8) Å, b_o = 5.77524(8) Å and c_o = 8.14033(6) Å] was obtained by the joint refinement [Figure 1E and F, Supplementary Table 1]. Notably, this space group is different from typical AFEs, such as $PbZrO_3$ (*Pbam*)[31], $AgNbO_3$ (*Pmc*2_1)[32] and $NaNbO_3$ (*Pbcm*)[33]. As shown in Figure 1E, there are two perovskite cells (dashed line) stacked along the c_o-axis, coupled with the $a^-a^-c^0$ oxygen octahedral tilting. Such a phenomenon is directly related to the commensurate structure corresponding to the ½(ooo)$_p$ reflections in Figure 1B and Supplementary Figure 1A. From the top view [Figure 1F], it is clear that the titling of the two adjacent octahedra (as indicated by the yellow arrows) are in the opposite direction. Therefore, this commensurate structure arose from the coupling between the atomic displacement and the octahedral titling.

In a perovskite structure, the electric polarization can be estimated by:

$$\boldsymbol{P} = \sum_{i} \frac{\boldsymbol{\delta_{Z_i} q_i}}{\boldsymbol{V}}$$

where δ_{Zi} is the polar displacement of the A- or B-site (shown in Supplementary Figure 3A) defined as the shift between the cations and the centroid of the oxygen polyhedral, q_i is the chemical valence of the cations and V is the unit cell volume of the perovskite. Supplementary Figure 3B shows the polarization component along $[110]_p$ and $[001]_p$ directions. The 3D dipole configuration, merged by different polarization components, is shown in Figure 2B and the corresponding stacked perovskite cells are presented in Figure 2A. Interestingly, electric dipoles with different orientations align along the $[001]_p$ direction [Figure 2B], resulting in a canting arrangement. Different from pure AFE $PbZrO_3$ [Supplementary Figure 4], in which the polarization only aligns in the a_p-b_p plane, PLZST shows not only an in-plane AFE characteristic, but also an out-of-plane FE characteristic along the $[001]_p$ direction. The projection of electric dipoles is antiparallel (AFE characteristic) in the $(001)_p$ plane (given in gray) and parallel (FE characteristic) in the $(110)_p$ plane (given in orange). The polarization component along the $[110]_p$ direction is only ~2 μC/cm² for PLZST, which is smaller than the local polarization in a perovskite unit of prototype $PbZrO_3$ (~26 μC/cm²) (calculated based on ref.[31]). Furthermore, a larger value of 7.9 μC/cm² is observed along the $[001]_p$ direction, resulting in a net polarization along the $[001]_p$ direction. Therefore, the polarization of PLZST has a significant local FE component, which is different from traditional AFEs. It is noteworthy that the local FE component has been discovered in several electric dipole configurations[15-18], which act as bridges between the classical AFE and FE states. These are the result of the competition between the FE and AFE orderings, which can lead to different incommensurate and commensurate transition routes.

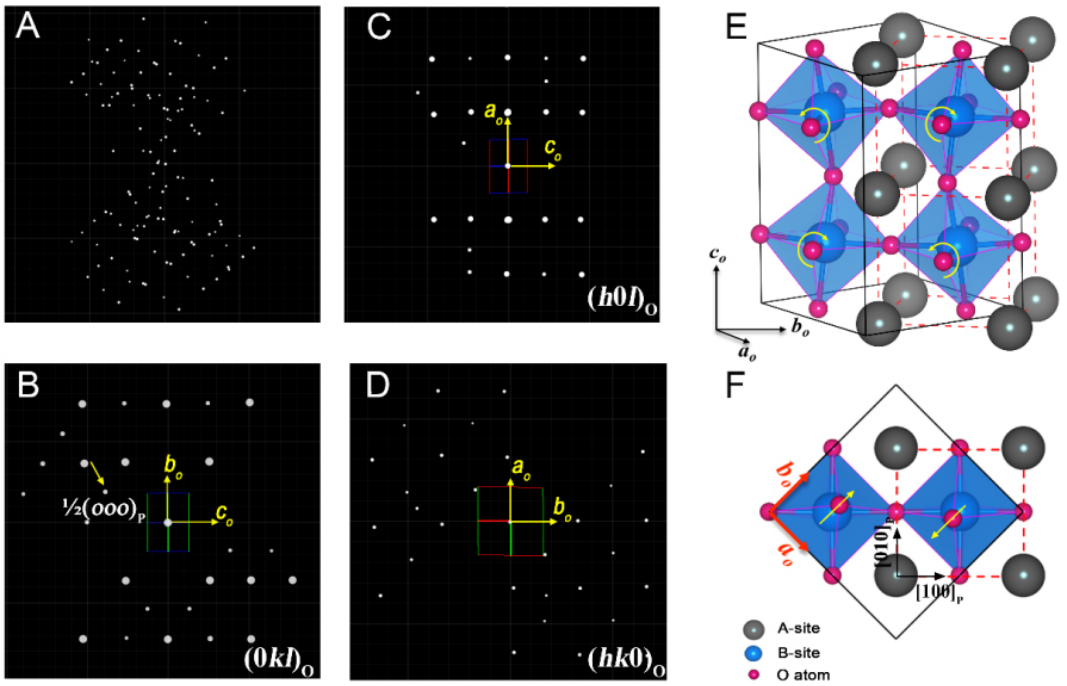

Figure 1. (A-D) Overview and representative reflection plane patterns. The reflection peaks marked by the yellow arrow in (B) arise from the commensurate structure along the $[001]_P$ direction. (E, F) Crystal structure of PLZST and the geometry relationship between the orthorhombic unit cell (solid black line) and the perovskite lattice (dotted black line). Subscripts O and P denote the orthogonal and perovskite lattices, respectively. PLZST: $(Pb_{0.91}La_{0.06})(Zr_{0.42}Sn_{0.40}Ti_{0.18})O_3$.

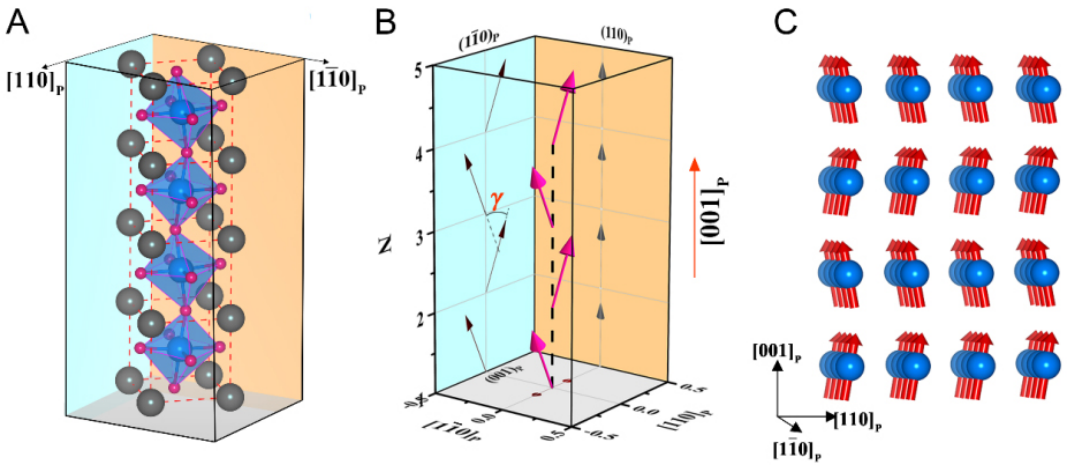

Figure 2. Canting polarization configuration in PLZST. (A) Schematic diagram of *ap* × *bp* × 4*cp* perovskite cells. (B) Spatial electric dipole configuration corresponding to the stacked perovskite cells in A. (C) Schematic of the arrangement of electric dipoles corresponding to 4 × 4 × 4 perovskites cells. The γ in the projection of the $(110)_p$ plane indicates the canting angle. Subscripts O and P denote the orthogonal and perovskite lattices, respectively. PLZST: $(Pb_{0.91}La_{0.06})(Zr_{0.42}Sn_{0.40}Ti_{0.18})O_3$.

The dipoles of two adjacent perovskite cells are arranged at a fixed angle γ of 27.5° in the $(110)_p$ plane (given in cyan). Figure 2C shows the arrangement of the electric dipole matrix. In analogy with the canting AFM structure, this arrangement of polarization can be termed as a new "canting AFE structure", whose angle γ is the so-called "canting angle". When γ equals 0° or 180°, a typical FE or AFE state occurs, respectively.

These results lead to a new question, how does the canting electric dipole configuration respond to an external electric field? The *P-E* and *S-E* hysteresis of PLZST are shown in Figure 3A. To reveal the evolution of the electric dipole configuration under the applied electric field, *in-situ* SXRD was performed. Interestingly, no phase transition can be observed according to the diffraction data [Supplementary Figure 5]. This is completely different from those AFE materials showing a large polarization hysteresis, which is ascribed to the electric field-induced phase transition[15,34,35]. No phase transition is the fundamental reason for the extremely small hysteresis of the present PLZST [Figure 3A].

To further reveal the electric dipole evolution as a function of the electric field, the structural refinement against *in-situ* diffraction patterns was adopted by using the single orthorhombic model. As shown in Figure 3B, the lattice expands continuously along the c_o-axis direction, i.e., the c_p direction, which displays a similar shape to the macroscopic *S-E* loop. In particular, the lattice strain at 6 kV/mm (0.07%) is very close to the measured macroscopic strain (0.075%), suggesting that the macroscopic strain mainly comes from the intrinsic lattice strain. In order to reveal the dipole configuration under different electric fields, the polarization under three electric fields, 0 kV/mm, 3 kV/mm and 6 kV/mm, were calculated based on the Rietveld refine results (shown in Supplementary Tables 2-4). Figure 3C shows the polarization as a function of the electric field. Interestingly, the value of polarization grows in the $[001]_p$ direction but fades in the $[110]_p$ direction. For example, along the $[001]_p$ direction, the polarization increases from 8.4 μC/cm² at 0 kV/mm to 23.2 μC/cm² at 6kV/mm, while along the $[110]_p$ direction, it reduces from 2.1 μC/cm² at 0 kV/mm to 0.5 μC/cm² at 6 kV/mm. Simultaneously, the canting angle γ decreases from 27.6° at 0 kV/mm to 2.7° at 6 kV/mm [Figure 3D]. The present result shows that the polarization rotates continuously to the $[001]_p$ direction driven by the electric field.

Figure 3E-G shows the electric field-induced evolution of the canting AFE structure more intuitively. It is interesting to see that the configuration of the electric dipoles evolves from a "canting" state to a "parallel" one by loading the electric field, leading to lattice strain along the c_o-axis (as shown in Figure 3B). Note that such continuous rotation of the dipoles as a function of the external field could be a general role in such dielectric and magnetic functional materials, such as electric field-driven polarization rotation in high-performance piezoelectrics[36] and magnetic field-driven spin moment rotation in the giant magnetostriction of $La(Fe_{11.5}Al_{1.5})$[13,37].

As a comparison, the antiparallel dipole ordering of prototype $PbZrO_3$ is shown in Supplementary Figure 4. There is a significant difference in the electric dipole configuration between PLZST and $PbZrO_3$. In a classical AFE material, the adjacent polarization orientation of electric dipoles should be aligned in the same direction under the electric field. It is without a doubt that strictly antiparallel aligned dipoles hinder the process of polarization rotation or switching. This is why the critical electric field of pure $PbZrO_3$ is too high to obtain a typical hysteresis loop. A similar situation exists in AFE $NaNbO_3$[38]. Recent studies have shown that AFEs with a non-antiparallel characteristic always have a lower critical field[15,16]. In contrast, compared to the dipole jump induced by the phase transition in some $PbZrO_3$-based AFEs, continuous rotation of electric dipoles in the present PLZST results in a slim *P-E* loop with a very small hysteresis. These findings are significant for the understanding of the relationship between the critical electric field and polarization configuration.

Various chemical compositions with different La contents

$Pb_{1-1.5x}La_x(Zr_{0.42}Sn_{0.40}Ti_{0.18})O_3$ (x = 0.03, 0.04, 0.05 or 0.06) compositions were also studied in this work (as seen in Supplementary Figure 6). A phase transition from FE to AFE with increasing La content indicates that La can weaken the FE and strengthen the AFE. When the content of La is greater than 0.05, the relaxation is

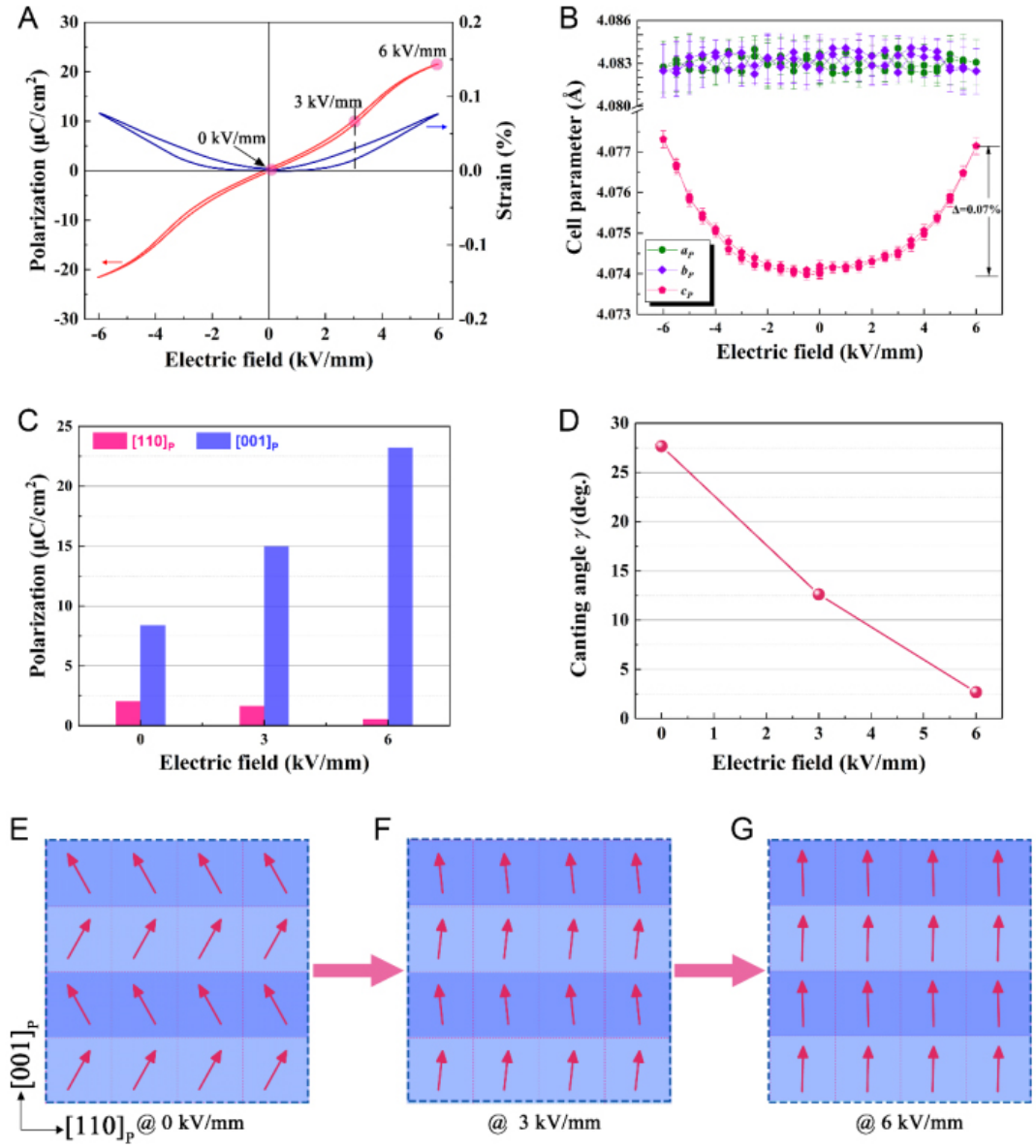

Figure 3. (A) *P-E* and *S-E* loops of PLZST. The dotted straight line shows the inflection point as a guide for the eye. (B) Evolution of perovskite cell parameters as a function of the bipolar electric field. (C) Polarization components along with the $[110]_P$ and $[001]_P$ directions at various electric fields. (D) Canting angle γ as a function of electric field. (E-G) Schematic of electric dipole map at different electric field conditions. The arrows represent the electric dipoles and the grid represents a perovskite unit. Subscript P denote the perovskite lattice. PLZST: $(Pb_{0.91}La_{0.06})(Zr_{0.42}Sn_{0.40}Ti_{0.18})O_3$.

significantly enhanced and the AFE is weakened. This result shows that La and Pb have an opposite influence on FE/AFE control due to the difference in ion radius and electronic polarizabilities between them[39]. The Pb(II) lone-pair electrons enhance the ferroelectricity, but La(III), which does not have lone-pair electrons, will weaken this influence, i.e., the doping of La breaks the long-range order constructed by Pb.

Additional insights into the physical polar structure of the slim hysteresis loop were obtained through phase-field simulations. The theoretical equations and parameter coefficients of the phase-field simulations are shown in Supplementary Table 5. As shown in Figure 4A, we calculated the antiparallel dipole

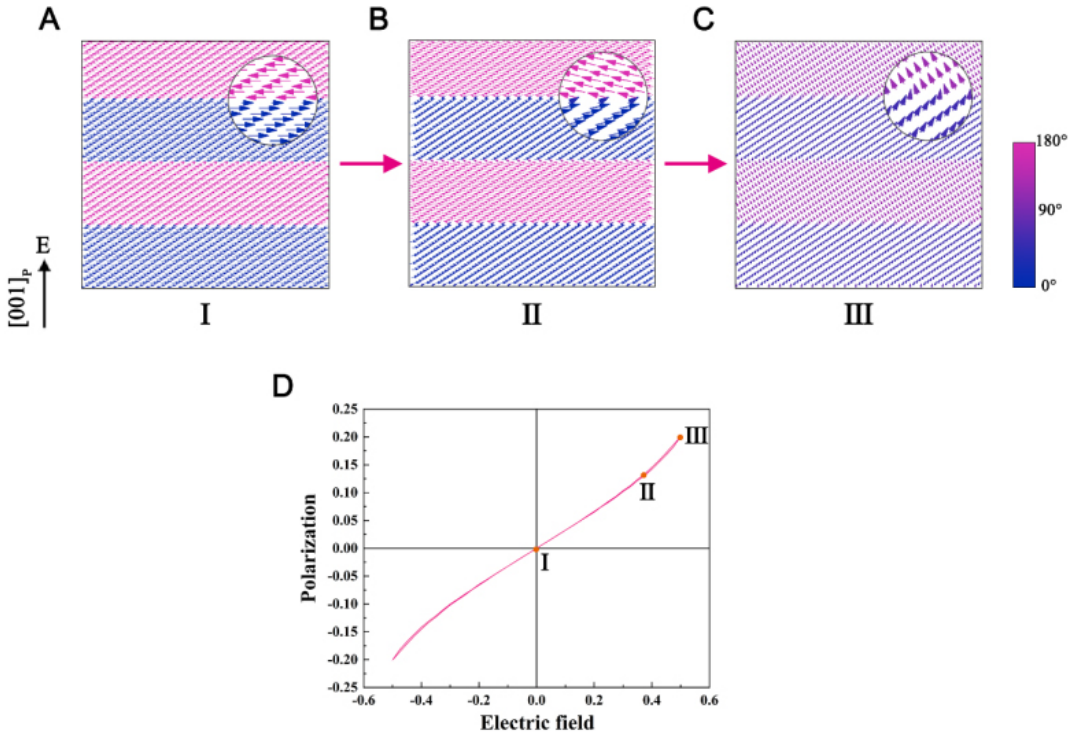

Figure 4. (A-C) Phase-field simulated snapshots, corresponding to the three dots I to III of the *P-E* loop and the polarization switching process of $Pb(Zr,Ti)O_3$. The right polarization direction is defined as 0°. (D) Calculated *P-E* loop. Subscript P denote the perovskite lattice.

configuration, which shows a typical AFE feature similar to pure $PbZrO_3$. The upward direction was defined as $[001]_P$, which is also the direction for electric field loading. Driven by an electric field, an obvious polarization rotation can be triggered. The dipoles gradually rotate to the electric field direction in Figure 4B and C, resulting in the antiparallel-to-canting transformation of the dipole configuration. This process is similar to the result of the experiment [Figure 3]. Intriguingly, the corresponding slim *P-E* loop [Figure 4D] was also calculated, which is entirely consistent with the experimental result [Figure 3A]. The result of the phase-field simulations indicates that the low electric field-induced antiparallel-to-canting transformation and the continual rotation of polarization can result in a slim hysteresis, which is consistent with the *in-situ* high-energy SXRD results.

CONCLUSION

In summary, an unprecedented canting electric dipole configuration has been revealed in $PbZrO_3$-based perovskites, which is a coexistence of the antiparallel AFE and the parallel FE ordering. Ascribed to the coupling between the distortion and the tilting of oxygen polyhedra, the electric dipoles were staggered along the $[001]_P$ direction in a canting manner. Different from the prototype AFE $PbZrO_3$, a strong FE component of 7.9 μC/cm² in the $[001]_P$ direction and a weak antiparallel component of 2 μC/cm² in the $[110]_P$ direction was observed in PLZST, resulting in a local net FE polarization. More intriguingly, it was found that polarization continuously rotates under loading electric fields. As a result, the AFE characteristic weakened while the FE characteristic enhanced. Such unique polarization evolution contributed to a small hysteresis of the *P-E* loop, which is consistent with the phase-field simulation results. It also resulted in an intrinsic lattice strain, which is equivalent to the macroscopic strain. The present work enriches the types of polarization configuration, which advances the understanding of AFE materials.

DECLARATIONS

Acknowledgments

The high-resolution synchrotron X-rays diffraction was collected on the BL44B2 beamline of SPring-8 with the approval of the Japan Synchrotron Radiation Research Institute. The high-resolution neutron diffraction was collected by Dr. Chin-Wei Wang at the National Synchrotron Radiation Research Center. The use of the Advanced Photon Source at Argonne National Laboratory was supported by the U.S. Department of Energy, Office of Science, Office of Basic Energy Sciences, under Contract No. DE-AC02-06CH11357. We thank Dr. Qingzhen Huang (NIST Center for Neutron Research, National Institute of Standards and Technology) for the useful discussion.

Authors' contributions

Experiment, characterization, writing original draft: Gao B
Review & editing, supervision: Liu H, Qi H
Methodology and software: Zhou Z, Sun J
Phase-field simulation: Xu K, Huang H
Selective area electron diffraction data acquisition: Deng S
High-energy in situ synchrotron X-ray diffraction data acquisition: Ren Y
Conceptualization, review, supervision: Chen J

Availability of data and materials

The *in-situ* experimental methods, data analysis procedures, details of the phase-field simulation, and supplementary figures are provided in Supplement Information.

Financial support and sponsorship

This work was supported by the National Natural Science Foundation of China (Grant Nos. 21825102, 22090042, and 22075014), the Fundamental Research Funds for the Central Universities, China (06500162, and 06500145).

Conflicts of interest

All authors declared that there are no conflicts of interest.

Ethical approval and consent to participate

Not applicable.

Consent for publication

Not applicable.

REFERENCES

1. Lawes G, Harris AB, Kimura T, et al. Magnetically driven ferroelectric order in $Ni_3V_2O_8$. *Phys Rev Lett* 2005;95:087205. DOI PubMed
2. Gareeva Z, Zvezdin K, Pyatakov A, Zvezdin A. Novel type of spin cycloid in epitaxial bismuth ferrite films. *Journal of Magnetism and Magnetic Materials* 2019;469:593-7. DOI
3. Nanda KK, Addison AW, Sinn E, Thompson LK. Helical antiferromagnetic copper(II) chains with a collagen structural motif. *Inorg Chem* 1996;35:7462. DOI PubMed
4. Cohen RJ. Canted ground states and the paramagnetic-antiferromagnetic transition in semiconductor zinc-blende antiferromagnets. *Phys Rev B Condens Matter* 1993;48:12813-6. DOI PubMed
5. Semitelou J, Yakinthos J. The conical magnetic structure of Dy_5Si_3. *Journal of Magnetism and Magnetic Materials* 2003;265:152-5.

DOI
6. Tokura Y, Seki S. Multiferroics with spiral spin orders. *Adv Mater* 2010;22:1554-65. DOI PubMed
7. Chung O, Kang W, Kim DL, Choi CH. Two rapid oscillations in the magnetoresistance in the field-induced spin-density-wave state of $(TMTSF)_2ClO_4$. *Phys Rev B* 2000;61:11649-55. DOI
8. Barker J, Tretiakov OA. Static and dynamical properties of antiferromagnetic skyrmions in the presence of applied current and temperature. *Phys Rev Lett* 2016;116:147203. DOI PubMed
9. Legrand W, Maccariello D, Ajejas F, et al. Room-temperature stabilization of antiferromagnetic skyrmions in synthetic antiferromagnets. *Nat Mater* 2020;19:34-42. DOI PubMed
10. Tegus O, Brück E, Buschow KH, de Boer FR. Transition-metal-based magnetic refrigerants for room-temperature applications. *Nature* 2002;415:150-2. DOI PubMed
11. Chang CZ, Zhang J, Feng X, et al. Experimental observation of the quantum anomalous Hall effect in a magnetic topological insulator. *Science* 2013;340:167-70. DOI PubMed
12. Kainuma R, Imano Y, Ito W, et al. Magnetic-field-induced shape recovery by reverse phase transformation. *Nature* 2006;439:957-60. DOI PubMed
13. Song Y, Huang R, Liu Y, et al. Magnetic-field-induced strong negative thermal expansion in $La(Fe,Al)_{13}$. *Chem Mater* 2020;32:7535-41. DOI
14. Song Y, Sun Q, Xu M, et al. Negative thermal expansion in $(Sc,Ti)Fe_2$ induced by an unconventional magnetovolume effect. *Mater Horiz* 2020;7:275-81. DOI
15. Liu H, Zhou Z, Qiu Y, et al. An intriguing intermediate state as a bridge between antiferroelectric and ferroelectric perovskites. *Mater Horiz* 2020;7:1912-8. DOI
16. Ma T, Fan Z, Xu B, et al. Uncompensated polarization in incommensurate modulations of perovskite antiferroelectrics. *Phys Rev Lett* 2019;123:217602. DOI PubMed
17. Wei XK, Tagantsev AK, Kvasov A, Roleder K, Jia CL, Setter N. Ferroelectric translational antiphase boundaries in nonpolar materials. *Nat Commun* 2014;5:3031. DOI PubMed PMC
18. Fu Z, Chen X, Li Z, et al. Unveiling the ferrielectric nature of $PbZrO_3$-based antiferroelectric materials. *Nat Commun* 2020;11:3809. DOI PubMed PMC
19. Chaboussant G, Crowell PA, Lévy LP, Piovesana O, Madouri A, Mailly D. Experimental phase diagram of $Cu_2(C_5H_{12}N_2)_2C_{l4}$: a quasi-one-dimensional antiferromagnetic spin- Heisenberg ladder. *Phys Rev B* 1997;55:3046-9. DOI
20. Khalyavin DD, Johnson RD, Orlandi F, Radaelli PG, Manuel P, Belik AA. Emergent helical texture of electric dipoles. *Science* 2020;369:680-4. DOI PubMed
21. Wei XK, Jia CL, Du HC, Roleder K, Mayer J, Dunin-Borkowski RE. An unconventional transient phase with cycloidal order of polarization in energy-storage antiferroelectric $PbZrO_3$. *Adv Mater* 2020;32:e1907208. DOI PubMed
22. Viehland D, Forst D, Li J. Compositional heterogeneity and the origins of the multicell cubic state in Sn-doped lead zirconate titanate ceramics. *Journal of Applied Physics* 1994;75:4137-43. DOI
23. Cai Y, Phillipp F, Zimmermann A, Zhou L, Aldinger F, Rühle M. TEM study of superstructure in a perovskite lead lanthanum zirconate stannate titanate ceramic. *Acta Materialia* 2003;51:6429-36. DOI
24. Knudsen J, Woodward D, Reaney IM. Domain variance and superstructure across the antiferroelectric/ferroelectric phase boundary in $Pb_{1-1.5}xLax(Zr_{0.9}TiM_{0.1})O_3$. *J Mater Res* ;18:262-71. DOI
25. He H, Tan X. Electric-field-induced transformation of incommensurate modulations in antiferroelectric $Pb_{0.99}Nb_{0.02}[(Zr_{1}xSnx)_{1}yTiy]_{0.98}O_3$. *Phys Rev B* 2005. DOI
26. Maclaren I, Villaurrutia R, Peláiz-barranco A. Domain structures and nanostructures in incommensurate antiferroelectric $PbxLa_{1}x(Zr_{0.9}Ti_{0.1})O_3$. *Journal of Applied Physics* ;108:034109. DOI
27. Hu T, Fu Z, Chen X, et al. Hierarchical domain structures in $(Pb,La)(Zr, Sn, Ti)O_3$ antiferroelectric ceramics. *Ceramics International* 2020;46:22575-80. DOI
28. Bikyashev EA, Reshetnikova EA, Tostunov MI. La^{3+} effect on dipole ordering in $Pb_{1}xLax[Zr_{0.7}Sn_{0.2}Ti_{0.1}]_{[1-x/4]}O_3$ ($0 < x \leq 0.03$) solid solutions. *Inorg Mater* 2009;45:919-24. DOI
29. Xu Z, Feng Y, Zheng S, Jin A, Wang F, Yao X. Phase transition and dielectric properties of La-doped $Pb(Zr,Sn,Ti)O_3$ antiferroelectric ceramics under hydrostatic pressure. *Materials Science and Engineering: B* 2003;99:441-4. DOI
30. Chen X, Dong X, Wang G, Cao F, Hu F, Zhang H. Dielectric and ferroelectric properties of lanthanum-modified lead zirconate stannate titanate (42/40/18) ceramics. *J Am Ceram Soc* 2018;101:3979-88. DOI
31. Corker DL, Glazer AM, Dec J, Roleder K, Whatmore RW. A re-investigation of the crystal structure of the perovskite $PbZrO_3$ by X-ray and neutron diffraction. *Acta Crystallogr B Struct Sci* 1997;53:135-42. DOI
32. Yashima M, Matsuyama S, Sano R, Itoh M, Tsuda K, Fu D. Structure of ferroelectric silver niobate $AgNbO_3$. *Chem Mater* 2011;23:1643-5. DOI
33. Darlington CNW. An X-ray diffraction study of $AgNbO_3$ and comparison with $NaNbO_3$. *Powder Diffr* 1999;14:253-7. DOI
34. Mohapatra P, Fan Z, Cui J, Tan X. Relaxor antiferroelectric ceramics with ultrahigh efficiency for energy storage applications. *Journal of the European Ceramic Society* 2019;39:4735-42. DOI
35. Qi H, Zuo R, Xie A, et al. Ultrahigh energy-storage density in $NaNbO_3$-based lead-free relaxor antiferroelectric ceramics with nanoscale domains. *Adv Funct Mater* 2019;29:1903877. DOI

36. Liu H, Chen J, Fan L, et al. Critical role of monoclinic polarization rotation in high-performance perovskite piezoelectric materials. *Phys Rev Lett* 2017;119:017601. DOI PubMed
37. Song Y, Huang R, Zhang J, et al. The critical role of spin rotation in the giant magnetostriction of $La(Fe,Al)_{13}$. *Sci China Mater* 2021;64:1238-45. DOI
38. Vousden P. The structure of ferroelectric sodium niobate at room temperature. *Acta Cryst* 1951;4:545-51. DOI
39. Shannon RD, Fischer RX. Empirical electronic polarizabilities in oxides, hydroxides, oxyfluorides, and oxychlorides. *Phys Rev B* 2006:73. DOI